Journal of Catalysis **199,** 48–59 (2001)
doi:10.1006/jcat.2000.3121, available online at http://www.idealibrary.com on IDEAL®

Selective Oxidation of CO, over Supported Au Catalysts

R. J. H. Grisel and B. E. Nieuwenhuys

Leiden Institute of Chemistry, Department of Heterogeneous Catalysis and Surface Chemistry, Gorlaeus Laboratories, Leiden University, P.O. Box 9502, 2300 RA Leiden, The Netherlands
E-mail: nieuwe_b@chem.leidenuniv.nl

Received July 31, 2000; revised November 21, 2000; accepted November 23, 2000; published online March 7, 2001

The selective oxidation of CO on Au/Al_2O_3 and $Au/MO_x/Al_2O_3$ ($M = Mg, Mn$) in the presence of H_2 was studied. The addition of MgO and MnO_x improves the CO oxidation activity and selectivity towards CO_2. The beneficial effect of MgO can be ascribed to stabilization of small Au particles, which are intrinsically more active in CO and H_2 oxidation. MnO_x is thought to be able to supply the active O needed for CO oxidation. Au catalysts containing both MgO and MnO_x are extremely active in CO oxidation. In the presence of H_2 selectivity towards CO_2 higher than 0.90 was observed for $Au/MgO/Al_2O_3$ and $Au/MnO_x/MgO/Al_2O_3$ at 100°C and below. The H_2 oxidation at low temperature was affected by adsorbed CO. At temperatures above 50°C the thermal desorption rate of CO was large enough for H_2 oxidation to commence, implying a decrease in selectivity. Besides H_2, water was also found to have a pronounced effect on the CO oxidation rate even at room temperature. The effect of water is ascribed to a beneficial role of surface OH groups in CO oxidation.

Key Words: **CO; H_2; H_2O; (selective) oxidation; gold; metal oxides; model; FTIR.**

1. INTRODUCTION

The polymer electrolyte fuel cell (PEFC) can generate electricity without polluting the environment. In this system hydrogen is oxidized over Pt electrodes and electric energy is generated, with ideally the only reaction product being H_2O. The supply of hydrogen needed for operation can be produced from methanol (1, 2) or other fuels (2, 3), via direct partial oxidation, steam reforming, and/or water-gas shift reactions. In the ideal situation the product stream from these reactions consists of only CO_2 and H_2. However, usually the product stream contains also several vol% H_2O and about 1–2 vol% CO (4). Especially the presence of CO in the feed causes major problems in Pt-based fuel cells, since Pt is effectively poisoned by CO at the operating temperatures of, e.g., 60–100°C (5, 6). In addition, H_2 oxidation will compete with CO oxidation in gas steams comprising both compounds. Hence, there is an urgent need to find a way to remove CO selectively from the product stream.

Several papers related to this topic have already been published dealing with catalysts based on γ-Al_2O_3-supported noble metals, such as Pt (7–9), Ru and Rh (9, 10). CO conversion and selectivity towards CO_2 in the presence of H_2 over supported Pt catalysts were found to depend on the contact time, the $CO : O_2$ molar ratio, and the support used (7). An optimum in CO conversion and selectivity to CO_2 was found at 200–250°C (7, 8). At lower temperatures the CO oxidation was rather slow due to inhibition of oxygen adsorption by adsorbed CO (8). At temperatures above 200–250°C the selectivity decreased because thermal desorption of CO enabled H_2 oxidation. The addition of H_2 was found to enhance CO oxidation on Pt/Al_2O_3 (8). This was explained by interaction between surface OH groups and adsorbed CO resulting in formation of formate species on the support, leaving free Pt sites needed for dissociative adsorption of O_2 and subsequent reaction with adsorbed CO.

Highly dispersed Au on suitable metal oxides (MO_x) exhibits extraordinarily high activity in low-temperature CO oxidation (11–13). Besides, several studies have indicated that the rate of CO oxidation over supported Au catalysts exceeds that of H_2 oxidation (13–15). This is a prerequisite for a catalyst to be able to oxidize CO selectively in H_2 rich gas flows. Generally, Au-based catalysts are considered to be superior to Pt-based catalysts because of their ability to oxidize CO selectively at high rates at temperatures corresponding to the operating temperature of the PEFC (14, 16, 17). Besides this, the catalysts studied were found to be insensitive to water and CO_2 in a wide range of concentrations (16). The CO oxidation rate over Au/α-Fe_2O_3 is even thought to be enhanced by the presence of H_2O (18). Similar to Pt based catalysts, the selectivity was found to decrease with increasing temperature due to the competitive H_2 oxidation at elevated temperatures (14, 16, 17).

In this study the effects of MgO and MnO_x on the CO oxidation activity over Au/Al_2O_3 have been investigated, as well as the influence of H_2 and H_2O. Two models, describing the CO oxidation in the absence and presence of H_2 will be discussed.

0021-9517/01 $35.00

2. EXPERIMENTAL

2.1. Catalyst Preparation

γ-Al_2O_3 (Engelhard Al-4172 P, ca. 200 m^2 g^{-1}, V_p ca. 2.8 ml g^{-1}) was used as support. Supported MO_x/Al_2O_3 catalysts (M = Mg, Mn) were prepared via pore volume impregnation. Dried γ-Al_2O_3 was placed in a flask under vacuum. $M(NO_3)_n \cdot mH_2O$ was dissolved in a quantity of demineralized water corresponding to the pore volume of the support used and added to the support under vacuum with an injection syringe at room temperature. After the pores of the support had taken up the solution, air was admitted into the flask. After the external edges had dried under ambient conditions the sample was further dried in air at 80°C for at least 16 h. Subsequently the sample was heated to 400°C (heating rate 5°C min^{-1}) in a flow of O_2 and kept at this temperature for 2 h.

Au was added to Al_2O_3 and MO_x/Al_2O_3 via homogeneous deposition precipitation (HDP) using urea as precipitating agent (19). An aqueous solution of $HAuCl_4 \cdot 3H_2O$ (99.999%) was used as Au precursor. The suspension was kept at 70°C under vigorous stirring to ensure a slow and gradual increase of the pH. At pH 8 the suspension was filtered and washed thoroughly with demineralized water to remove Cl^-, which may have a detrimental effect on the oxidation of CO (11–13). The samples were kept under ambient conditions until the external edges had dried. Finally, the samples were dried overnight in air at 80°C and subsequently heated to 300°C (heating rate 5°C min^{-1}) in a flow of O_2. The samples were kept at this temperature for 2 h. To test the reproducibility of this method two similarly prepared Au/Al_2O_3 catalysts were characterized and tested ($Au(a)/Al_2O_3$ and $Au(b)/Al_2O_3$).

$Au/MnO_x/MgO/Al_2O_3$ was prepared by adding Mn to calcined $Au/MgO/Al_2O_3$. HDP was employed since pore volume impregnation was found to have a disadvantageous effect on the average Au particle size under the applied conditions. The resulting catalyst was treated similarly to other Au containing catalysts. The supported Au catalysts had an intended Au loading of 5 wt% and an Au : M atomic ratio of 1 : 5. The intended Au : Mn : Mg atomic ratio was 1 : 5 : 5 in the case of $Au/MnO_x/MgO/Al_2O_3$.

2.2. Catalyst Characterization

The Au loading was verified with atomic absorption spectroscopy (AAS) using a Perkin–Elmer 3100 with an air/acetylene flame. The catalysts were dissolved in hot aqua regia. After cooling, the solutions were diluted with demineralized water. Parts of the undissolved support were allowed to settle before actual analysis.

To obtain information about the identity of the metal (oxide) phases present on the catalyst, X-ray diffraction (XRD) was employed. The average Au particle size was estimated from XRD line broadening using Scherrer's equation (20). The diffractograms were recorded on a Philips PW 1050/25 diffractometer, equipped with a Cu$K\alpha$ X-ray source ($\lambda = 0.15418$ nm) operating at 50 kV and 40 mA.

To obtain information on the particle size distribution, the catalysts were subjected to a detailed high-resolution transmission electron microscopy (HRTEM) study. The HRTEM measurements were performed on a Philips CM30UT electron microscope equipped with a LaB_6 filament as the source of electrons operated at 300 kV. The samples were mounted on a micro-grid carbon polymer supported on a copper grid by placing a few droplets of a suspension of ground catalyst in ethanol on the grid, followed by drying at ambient condition. Maximum resolution was 0.5 nm at 500 k magnification. From each catalyst about 300 particles were measured to determine a statistically justified average particle size and particle size distribution. Elemental analysis was performed with energy dispersive X-ray analysis (EDX), by means of a built-in LINK EDX system to monitor possible contaminations in the catalyst.

2.3. Activity Measurements

Oxidation measurements were performed in a lab-scale flow reactor. In each experiment 0.20 g catalyst was used. Before measurement the catalyst was pre-reduced *in situ* in 4 vol% H_2 in He at 300°C for 30 min. Before the reactants were admitted the reactor was purged with He at room temperature. The reactant flow consisted of a mixture of either CO and O_2 (ratio unity), H_2 and O_2 (ratio 4 : 1), or H_2, CO, and O_2 (ratio 4 : 2 : 1). The total concentration of reactants in the feed was always 4 vol% balanced in He. A total gas flow of 40 ml min^{-1} was applied corresponding with a GHSV of about 2500 h^{-1}. The reaction was temperature programmed between 25 and 400°C with a heating (and cooling) rate of 5°C min^{-1}. Two reaction cycles, each consisting of a heating and a cooling curve, were recorded to monitor possible hysteresis or catalyst deactivation. Online gas analysis was performed with a Chrompack CP-2002 gas chromatograph equipped with a Molsieve 5 Å column to detect CO, O_2 and H_2 and a Hayesep A column for CO_2.

The conversion is defined as the amount of mol CO (H_2) oxidized divided by the total amount of CO (H_2) fed to the catalyst. In CO and H_2 containing mixtures the selectivity towards CO_2 (S^{CO2}) is defined as the ratio of O_2 used for the CO oxidation reaction over the total O_2 consumption. All activities of the different catalysts at a temperature T are compared per gram catalyst.

2.4. Fourier Transform Infrared Spectroscopy

The catalysts were also investigated with Fourier transform infrared spectroscopy (FTIRS). For that purpose the catalysts were pressed into thin self-sustaining discs

and mounted in a sample holder, which was placed in a vacuum cell. The base pressure of the system was about 5×10^{-6} mbar. The samples were pretreated in either 100 mbar O_2 (99.998%) or 100 mbar H_2 (99.999%) at 300°C for 30 min. Subsequently, the cell was evacuated and cooled to room temperature. Before admission of the gases a background spectrum was recorded which was subtracted. The spectra were corrected for gas phase CO. The FTIRS measurements were performed on a Mattson Galaxy 2020 spectrophotometer, which operated with a resolution of 2 cm^{-1}. Each spectrum is an average of 50 consecutive scans.

3. RESULTS

3.1. Catalyst Characterization

XRD was used to estimate the average Au particle size (Table 1) and to identify the crystalline phases present on the catalyst. For all catalysts a maximum in reflection was detected at $d = 2.355$ Å, which is characteristic of metallic Au. In case of catalysts containing Mn a weak diffraction peak was also observed for $d = 2.487$ Å. The formal oxidation state of Mn could not be identified unambiguously. Presumably MnO_x on the surface of the catalyst is present as a mixture of oxides (21).

The catalytic activity of supported Au catalysts strongly depends on the Au particle size (22–25). Therefore, it is of utmost importance to study the Au particle size and size distribution in more detail with, e.g., HRTEM. The particle size distributions of $Au/MnO_x/Al_2O_3$, $Au/MgO/Al_2O_3$, and $Au/MnO_x/MgO/Al_2O_3$ are shown in Fig. 1.

It was found very difficult to reproduce the preparation of small Au particles deposited on either Al_2O_3 or MnO_x/Al_2O_3. However, addition of MgO to Al_2O_3 resulted in good reproducibility of manufacturing catalysts with a highly dispersed Au phase with a narrow particle size distribution. For most catalysts the average HRTEM Au particle size agreed with those determined from XRD line broadening (Table 1). According to XRD, depositing Au onto MnO_x/Al_2O_3 yielded catalysts with relatively big Au crystallites. This was experimentally affirmed with HRTEM. The Au particle size distribution was broad (Fig. 1a), and also large patches of Mn-rich material were observed. In case of $Au/MgO/Al_2O_3$ few larger Au crystallites were observed, but they constituted the minority of the metal particles (Fig. 1b). EDX analysis spectra were not easy to

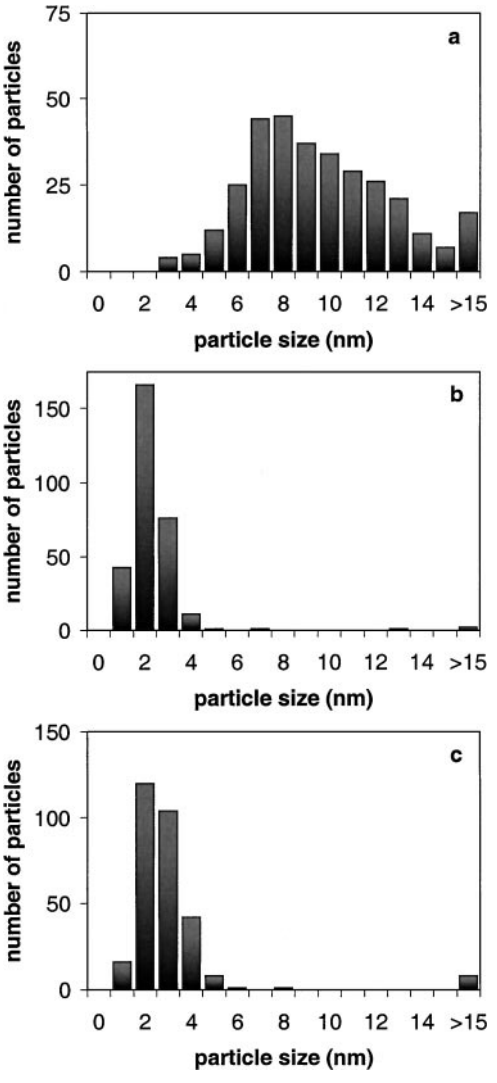

FIG. 1. Particle size distribution of (a) $Au/MnO_x/Al_2O_3$, (b) $Au/MgO/Al_2O_3$, and (c) $Au/MnO_x/MgO/Al_2O_3$ determined with HRTEM.

TABLE 1

Au Loading (AAS) and Average Au Particle Size (XRD, HRTEM)

Catalyst	Au loading (wt %)	Average Au particle size (nm)		Fraction of Au atoms[a] at	
		XRD	TEM	Surface	Interface
$Au(a)/Al_2O_3$	5.0	3.1	3.6 ± 1.4	0.42	0.09
$Au(b)/Al_2O_3$	5.1	10.1	8.7 ± 3.2	0.18	0.01
$Au/MnO_x/Al_2O_3$	4.8	9.8	9.2 ± 2.7	0.17	0.01
$Au/MgO/Al_2O_3$	5.0	2.1	2.2 ± 1.0	0.60	0.20
$Au/MnO_x/MgO/Al_2O_3$	4.9	17.4	2.7 ± 1.0	0.51	0.14

[a] Determined from HRTEM data, assuming a hemispherical particle size.

interpret as the signal for Mg partly overlaps the signal of Al. However, MgO was not observed as a separate phase in the HRTEM images, indicating possible high dispersion of Mg over Al_2O_3. Although from XRD line-broadening a rather large average Au particle size was expected for $Au/MnO_x/MgO/Al_2O_3$ also (Table 1), HRTEM shows that in addition to these large metal particles numerous small particles were also present (Fig. 1c). These small particles give such a large line broadening that they easily escape detection with XRD. In addition to the Au particles, patches of Mn-rich material were also observed for this catalyst. Oxidation experiments, performed at moderate temperatures ($T < 400$°C), did not influence the catalyst morphology significantly. Additional elemental analysis provided no indication of either Cl^- contamination or the presence of other impurities.

3.2. CO Oxidation in Oxidizing Environment ($CO : O_2 = 1 : 1$)

CO oxidation was carried out in excess oxygen. Two consecutive reaction cycles, each consisting of one heating and one cooling stage, were monitored. An example is given in Fig. 2a. The CO conversion during the first heating stage is somewhat higher than during the following runs. The second heating curve was found to be more representative for the intrinsic activity of the different catalysts and was thus used for comparison of catalysts. Repeated heating and cooling cycles were very similar to those of the second heating runs shown in Fig. 2b.

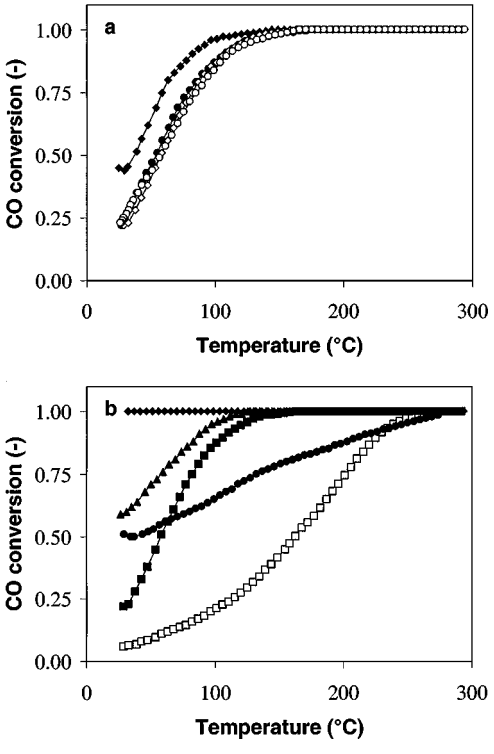

FIG. 2. CO conversion versus temperature (°C) of (a) $Au(a)/Al_2O_3$; first heating (◆), first cooling (●), second heating (◇), and second cooling curve (○); and (b) second heating curves of $Au(a)/Al_2O_3$ (■), $Au(b)/Al_2O_3$ (□), $Au/MnO_x/Al_2O_3$ (●), $Au/MgO/Al_2O_3$ (▲), and $Au/MnO_x/MgO/Al_2O_3$ (◆).

The CO oxidation activities are summarized in Fig. 2b. As can be seen, $Au(a)/Al_2O_3$ and $Au(b)/Al_2O_3$ are only moderately active at 50 and 150°C, respectively, whilst the other Au-containing catalysts exhibit high activity even at room temperature. This result complicates the determination of intrinsic kinetics of CO oxidation over these catalysts. Therefore, the trend in activity at room temperature will be mainly used to compare the behavior of the catalysts. The CO oxidation activity ($g_{cat.}^{-1}$) decreased in the following order: $Au/MnO_x/MgO/Al_2O_3 \gg Au/MgO/Al_2O_3 > Au(a)/Al_2O_3 > Au/MnO_x/Al_2O_3 \gg Au(b)/Al_2O_3$ (Fig. 2b). The number of Au atoms exposed to the gas phase was calculated from the Au particle size as determined with HRTEM and the actual Au loading obtained by AAS (Table 1). We assume that all Au particles are hemispherical.

To investigate the possible effect of catalyst pretreatment, CO oxidation activity measurements were also carried out after *in situ* oxidation of the catalysts in 4 vol% O_2 in He at 300°C for 30 min. Generally, the activity of these pre-oxidized samples was lower during the first heating stage than in the following stages. Apparently the catalyst needs to be activated in the presence of a reducing species (CO) at elevated temperatures. Similar results were found by Dekkers *et al.* (26, 27). After activation, i.e., during the second heating curve, the performance was still somewhat inferior to those of the pre-reduced samples.

3.3. Hydrogen Oxidation Experiments ($H_2 : O_2 = 4 : 1$)

H_2 oxidation was performed with surplus hydrogen. The maximum possible H_2 conversion was 0.5. The H_2 oxidation activity of $Au(a)/Al_2O_3$ is given in Fig. 3a. The catalyst's ability to oxidize CO more readily than H_2 is thought to be a prerequisite for selective CO oxidation in the presence of H_2 (14). As can be deduced from Figs. 2a and 3a, the capability of $Au(a)/Al_2O_3$ to catalyze the oxidation of CO at low temperature exceeds that of H_2 significantly after *in situ* reduction (first heating curve). In contrast with CO oxidation, a large hysteresis in H_2 oxidation activity was observed. In the cooling branch the temperature at which 45% of the admitted H_2 is consumed ($T_{45\%}$) was about 30°C lower than in the heating branch.

Figure 3b shows the second heating curves of H_2 conversion. Most catalysts indeed do show better performance in CO oxidation than in H_2 oxidation at ambient temperature (Tables 2, 3). An exception, however,

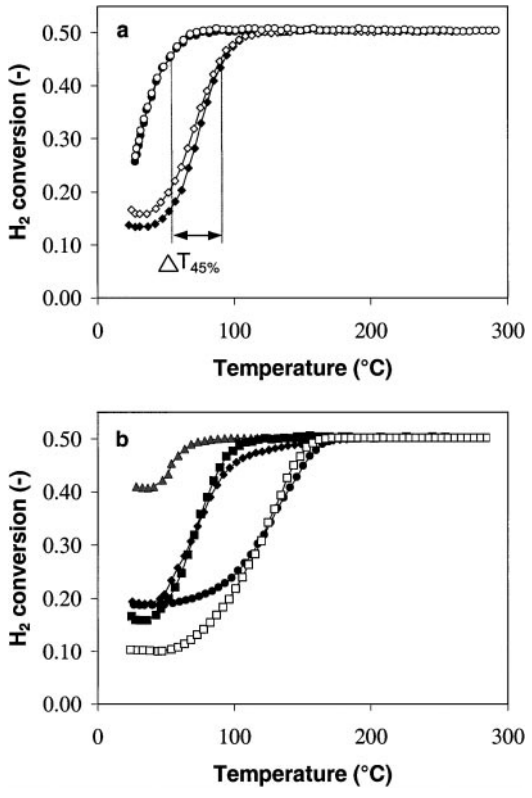

FIG. 3. H_2 conversion versus temperature (°C) of (a) $Au(a)/Al_2O_3$; first heating (◆), first cooling (●), second heating (◇), and second cooling curve (○); and (b) second heating curves of $Au(a)/Al_2O_3$ (■), $Au(b)/Al_2O_3$ (□), $Au/MnO_x/Al_2O_3$ (●), $Au/MgO/Al_2O_3$ (▲), and $Au/MnO_x/MgO/Al_2O_3$ (◆).

is the high activity in H_2 oxidation found for $Au/MgO/Al_2O_3$. The H_2 oxidation activity decreased in the following order: $Au/MgO/Al_2O_3 \gg Au/MnO_x/MgO/Al_2O_3 \approx Au(a)/Al_2O_3 > Au/MnO_x/Al_2O_3 > Au(b)/Al_2O_3$. Hysteresis was observed for all samples. Differences in $T_{45\%}$ during heating and cooling curves were approximately 30–40°C (Table 3). A larger hysteresis (55°C) was found for $Au/MnO_x/MgO/Al_2O_3$.

TABLE 2

Influence of Pretreatment on CO Oxidation Activity (Second Heating Curve)

Catalyst	Pre-reduced			Pre-oxidized		
	$\alpha(CO)^a$	$T_{50\%}{}^b$	$T_{95\%}{}^b$	$\alpha(CO)^a$	$T_{50\%}{}^b$	$T_{95\%}{}^b$
$Au(a)/Al_2O_3$	0.22	57	122	0.21	62	124
$Au(b)/Al_2O_3$	0.06	163	239	0.04	170	248
$Au/MnO_x/Al_2O_3$	0.49	35	258	0.37	74	299
$Au/MgO/Al_2O_3$	0.59	<25	99	0.47	39	120
$Au/MnO_x/MgO/Al_2O_3$	1.00	<25	<25	0.79	<25	59

[a] Determined room temperature (25°C).
[b] Temperature (°C) at 50% and 95% CO conversion.

TABLE 3

H_2 Oxidation over Supported Au Catalysts (Second Heating Curve)

Catalyst	$\alpha(H_2)^a$	$T_{25\%}{}^b$	$T_{45\%}{}^b$	$\Delta T_{45\%}{}^c$
$Au(a)/Al_2O_3$	0.16	63	91	38
$Au(b)/Al_2O_3$	0.10	108	143	31
$Au/MnO_x/Al_2O_3$	0.19	102	151	30
$Au/MgO/Al_2O_3$	0.41	<25	54	29
$Au/MnO_x/MgO/Al_2O_3$	0.19	57	99	55

[a] Determined at room temperature (25°C).
[b] Temperature (°C) at 25% and 45% H_2 conversion.
[c] Absolute difference in $T_{45\%}$ (°C) between heating and cooling curves.

3.4. Selective Oxidation of CO in the Presence of Hydrogen ($H_2 : CO : O_2 = 4 : 2 : 1$)

Figure 4 shows the conversion of CO over the different catalysts when H_2 is present in the reactant flow. At low temperature relatively high CO conversions were obtained, as was the case for activity measurements without H_2 in the feed. Hardly any H_2 was oxidized at 50–100°C. At higher temperatures, however, the CO conversion decreased, whereas the H_2 conversion increased. Depending on the composition of the catalyst, H_2 conversion exceeds that of CO at temperatures between 150 and 250°C. In the cases of $Au(b)/Al_2O_3$ and $Au/MnO_x/Al_2O_3$ CO conversion even drops to zero at around 250°C, while over $Au(a)/Al_2O_3$, $Au/MgO/Al_2O_3$, and $Au/MnO_x/MgO/Al_2O_3$ a considerable amount of CO is still being oxidized. At even higher temperatures (>300°C) the CO oxidation activity increases again at the expense of H_2 oxidation activity for all catalysts. None of the catalysts showed hysteresis in either CO or H_2 consumption; this is in contrast to H_2 oxidation in the absence of CO (Section 3.3).

Arrhenius plots of H_2 oxidation over the various catalysts in the presence of CO are shown in Fig. 5. From these the apparent activation energy (E_a) for H_2 oxidation was calculated at low conversion ($0.05 > \alpha > 0.25$). At low temperatures E_a is higher than at elevated temperatures (Table 4). The (reciprocal) temperature at which the inflection point in the Arrhenius curves was found to vary per catalyst. No inflection point was found for $Au/MnO_x/MgO/Al_2O_3$.

The only products detected were CO_2 and H_2O. No traces of CH_3OH or CH_4 were found. Additionally, the point of intersection between the CO and H_2 conversion curves was always found at conversions around 0.33 provided that all O_2 was consumed. This is to be expected from stoichiometry when to be the only processes to occur are considered to be the oxidation of CO and H_2. This excludes the presence of any compound in the product flow as a result from

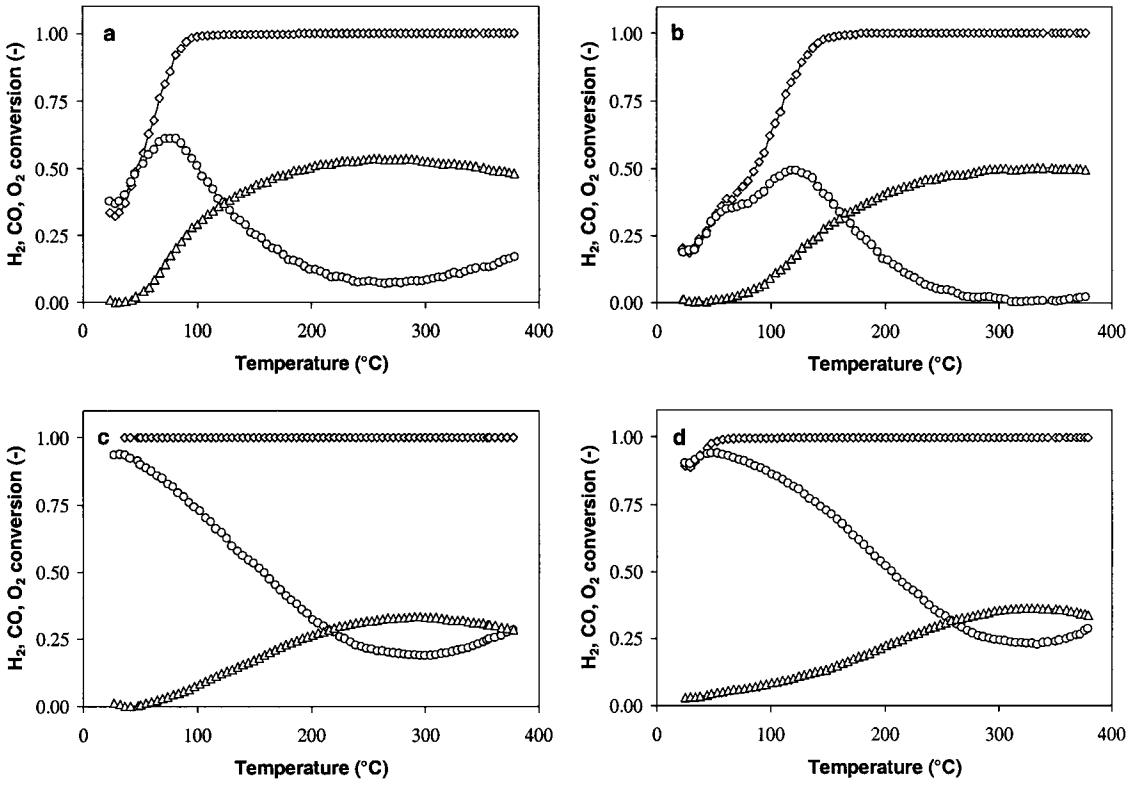

FIG. 4. Conversion of CO (○), H_2 (△), and O_2 (◇) versus temperature (°C) over (a) Au(a)/Al_2O_3, (b) Au/MnO_x/Al_2O_3, (c) Au/MgO/Al_2O_3, and (d) Au/MnO_x/MgO/Al_2O_3.

reactions between CO and H_2 in the temperature range studied.

3.5. Fourier Transform Infrared Spectroscopy (FTIRS)

Figure 6a shows the FTIR spectra of 25 mbar CO admitted at room temperature after oxidative (black lines) and reductive (gray lines) pretreatment. Generally, after reductive pretreatment the absorption maximum is at around 2100 cm^{-1}, which can be ascribed to the Au^0–CO bond (12, 27, 28). All CO absorption peaks show tailing towards lower wavenumbers (2075–2100 cm^{-1}). Upon admission of 25 mbar O_2, this tail disappears instantaneously, and the peak maximum shifts to higher wavenumbers. An example is given in Fig. 6b. The absorption peaks after oxidative pretreatment are much more diverse. Generally, the peak maxima were found at higher wavenumbers and are more scattered than after reductive pretreatment. Absorption maxima were between 2108 and 2146 cm^{-1}, the higher values representing $Au^{\delta+}$–CO (27, 29, 30). Here also tailing towards lower wavenumbers (2100–2135 cm^{-1}) was observed for Au(b)/Al_2O_3 and Au/MnO_x/Al_2O_3. The FTIR spectrum of CO on pre-oxidized Au(a)/Al_2O_3 even shows two distinct maxima at 2108 and 2127 cm^{-1}. The difference in peak intensity also is much more pronounced; e.g., hardly any peak was found for CO on Au/MnO_x/MgO/Al_2O_3 after oxidative pretreatment, whereas CO on pre-oxidized Au/MgO/Al_2O_3 gives the highest response. After addition of O_2 the spectra do not change as prominently as after reductive pretreatment (Fig. 6b). The tail diminished rather slowly at the cost of the peak maximum at higher wavenumbers. Accordingly, also the 2108 : 2127 cm^{-1} peak intensity ratio of Au(a)/Al_2O_3 declined after introduction of O_2.

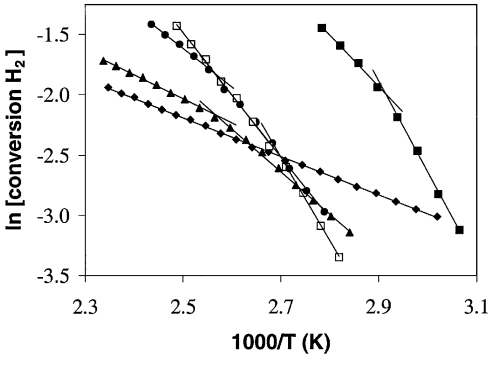

FIG. 5. Arrhenius plots of H_2 oxidation in a mixture of H_2, CO, and O_2 (4 : 2 : 1): Au(a)/Al_2O_3 (■), Au(b)/Al_2O_3 (□), Au/MnO_x/Al_2O_3 (●), Au/MgO/Al_2O_3 (▲), and Au/MnO_x/MgO/Al_2O_3 (◆).

TABLE 4

Kinetic Data for H_2 Oxidation in the Presence of CO + O_2

Catalyst	Inflection point (°C)[a]	$\alpha(H_2)$ at inf. point	α(CO) at inf. point	E_a [I][b] (kJ · mol^{-1})	E_a [II][b] (kJ · mol^{-1})
$Au(a)/Al_2O_3$	70	0.13	0.61	62	36
$Au(b)/Al_2O_3$	96	0.08	0.07	76	30
$Au/MnO_x/Al_2O_3$	117	0.16	0.49	42	27
$Au/MgO/Al_2O_3$	118	0.12	0.65	29	16
$Au/MnO_x/MgO/Al_2O_3$	—	—	—	—	14

[a] Temperature (°C) at which the E_a for H_2 oxidation changes.
[b] Calculated E_a (kJ · mol^{-1}) for the low-temperature (I) and high-temperature branch (II).

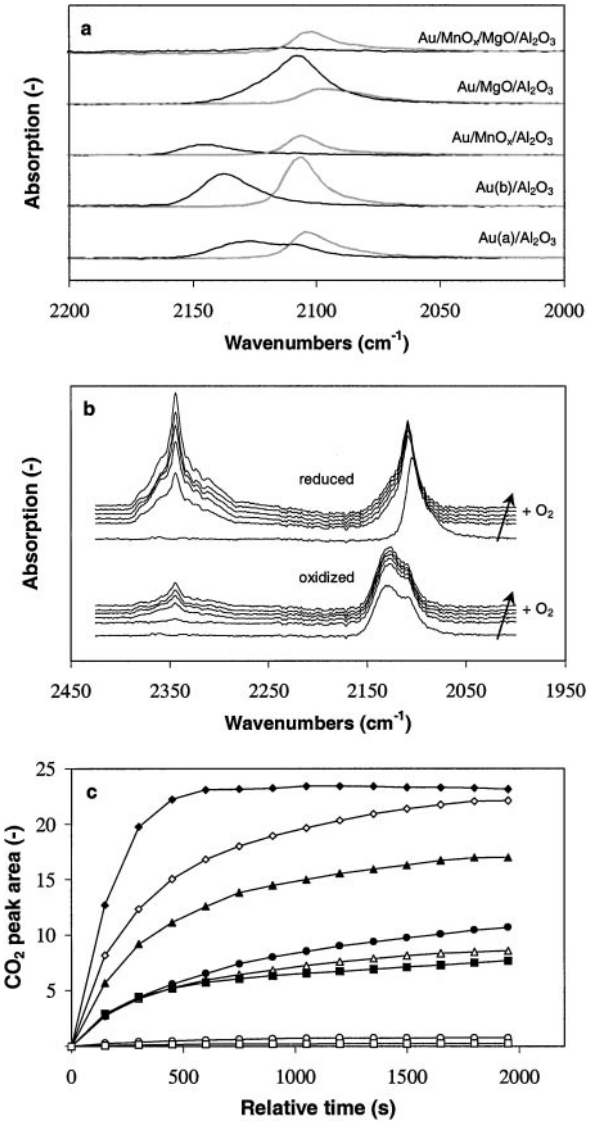

FIG. 6. FTIR spectra at 25°C of (a) 25 mbar CO on supported Au catalyst after reductive (gray lines) and oxidation pretreatment (black lines), and (b) $Au(a)/Al_2O_3$ after addition of 25 mbar O_2 (CO : O_2 unity). Time between consecutive spectra 2.5 min. (c) CO_2 peak area versus reaction time after reductive (closed symbols) and oxidative pretreatment (Open symbols) of $Au(a)/Al_2O_3$ (■), $Au/MnO_x/Al_2O_3$ (●), $Au/MgO/Al_2O_3$ (▲), and $Au/MnO_x/MgO/Al_2O_3$ (◆).

Since several of the catalysts are highly reactive even at room temperature it is hard to say much about the kinetics. Nevertheless, data collected from FTIRS do provide for a method to compare the initial CO oxidation rates. The area under the CO_2 peak, appearing in the FTIR spectra (2343 cm^{-1}) upon O_2 addition, is a measure of the extent of CO conversion. However, the formation of 'C'-species on the surface is thus not taken into consideration, although probably a significant amount of CO is being stored as such during reaction. It would be better to monitor the change in CO peak intensity. However, due to practical problems, such as excess adsorbates and gas-phase CO corrections, this was not possible. Figure 6c gives the integrated CO_2 peak areas as function of time for the different catalysts after both reductive and oxidative pretreatment. The initial CO oxidation activity can be characterized by $d(CO_2)_{area}/dt$ at $t = 0$ min (Table 5).

Similar experiments were carried out in the presence of H_2. First the sample was pretreated as described above. However, before either CO or O_2 was introduced, first 50 mbar of H_2 was admitted to the catalyst. Subsequently 25 mbar CO and 12.5 mbar O_2 were added, obtaining a $H_2 : CO : O_2$ ratio of 4 : 2 : 1. For all catalysts, the observed CO peak positions after both oxidative and reductive pretreatment in the presence of H_2 were nearly identical and

TABLE 5

CO-FTIRS Data of Supported Au Catalysts

	Oxidized		Reduced	
Catalyst	CO peak max. (cm^{-1})	Initial oxn. Activity[a]	CO peak max. (cm^{-1})	Initial oxn. Activity[a]
$Au(a)/Al_2O_3$	2108, 2127	0.7	2105	19.7
$Au(b)/Al_2O_3$	2138	0.1	2107	10.0
$Au/MnO_x/Al_2O_3$	2146	1.6	2106	18.2
$Au/MgO/Al_2O_3$	2108	16.8	2098	35.7
$Au/MnO_x/MgO/Al_2O_3$	2114[b]	52.4	2103	86.4

[a] Initial CO oxidation activity calculated from $d(CO_2)_{area}/dt$ at $t = 0$ (×1000).
[b] Very weak absorption peak.

roughly similar to those observed for CO on reduced samples without H_2 in the cell. The production of CO_2 in time, however, seems to be accelerating in the early stage of the reaction.

3.6. The Effect of H_2O on CO Oxidation Activity

Since the product stream inevitably contains significant amounts of H_2O, due to the reaction between H_2 and O_2 in the feed, it is important to study the effect of H_2O on the catalytic activity. For that purpose 50 μl of H_2O was added to the reactant gas with an injection syringe in a pre-heated chamber (120°C). Subsequently, the gas was cooled and led over the catalyst, which was kept at room temperature. The change in oxidation activity due to the presence of H_2O was monitored. Via several heating stages at 100, 200, and 300°C we tried to restore the original performance. Finally, a second amount of H_2O was injected to study the reproducibility of this phenomenon. The results of this study are summarized in Fig. 7. While the light gray bars in the graph correspond with the heating stages, the white areas represent CO conversion curves at room temperature. The encircled dark gray ellipses at 100 and 430 min emphasize the injection points of 50 μl H_2O. As shown in Fig. 7 the catalysts responded quite differently to the addition of H_2O. Whereas the activity of $Au/MgO/Al_2O_3$ and $Au/MnO_x/MgO/Al_2O_3$ is clearly enhanced and the performance of $Au(a)/Al_2O_3$ is only slightly improved, H_2O has a detrimental effect on the CO oxidation activity of $Au/MnO_x/Al_2O_3$. The effect of the different heating stages is also evident. The conversion curve of a catalyst after the different heat-treatments correlate to the activity of different "hydration grades" of that catalyst at ambient temperature. The CO conversions over the different catalysts at the individual stages are summarized in Table 6. From this it is also clear that only dehydration of $Au/MnO_x/Al_2O_3$ is beneficial for the CO oxidation activity, while all other catalysts lose some of their activity upon dehydration.

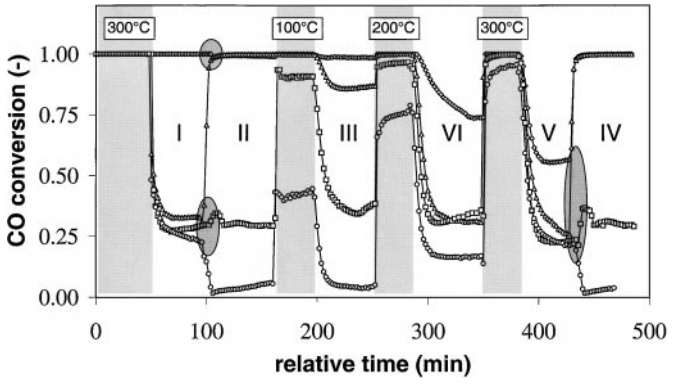

FIG. 7. CO conversion of $Au(a)/Al_2O_3$ (□), $Au/MnO_x/Al_2O_3$ (○), $Au/MgO/Al_2O_3$ (△), and $Au/MnO_x/MgO/Al_2O_3$ (◇). The white areas correspond to CO conversion at 25°C; the encircled gray ellipses represent injection points of 50 μl H_2O.

TABLE 6

Influence of H_2O on CO Oxidation Activity at Ambient Temperature

Catalyst	α(I)	α(II)[a]	α(III)	α(IV)	α(V)	α(VI)[a]
$Au(a)/Al_2O_3$	0.28	0.30	0.36	0.34	0.23	0.30
$Au(b)/Al_2O_3$	—	—	—	—	—	—
$Au/MnO_x/Al_2O_3$	0.24	0.04	0.03	0.17	0.21	0.04
$Au/MgO/Al_2O_3$	0.33	1.00	0.87	0.33	0.30	1.00
$Au/MnO_x/MgO/Al_2O_3$	1.00	1.00	0.99	0.74	0.56	1.00

[a] CO conversion at 25°C after injection of 50 μl H_2O.

4. DISCUSSION

4.1. Activity and Selectivity

In general, the TOF is a convenient parameter to compare the activity of catalysts. The active site(s) on supported Au catalysts have not yet been identified unambiguously. In addition, no suitable characterization technique is available to determine the Au dispersion. Consequently, the number of surface Au atoms must be estimated. It is often assumed that all Au particles are hemispherical, the atoms in the clusters are close-packed (fcc), i.e., particles without stress or strain, and the Au surface is not (partially) covered by MO_x, which is most probably not true for MnO_x. These assumptions may engender such severe uncertainties that the resulting TOFs are practically meaningless. Hence, the use of TOFs is insufficiently founded to compare the performance of different Au based catalysts. Therefore, in the present paper the TOF is not used to express catalytic activity.

Based on the variation of CO and H_2 conversion with increasing temperature (Fig. 2, 3, and 4) it is concluded that (i) the order of the catalysts in CO oxidation activity is $Au/MnO_x/MgO/Al_2O_3 \gg Au/MgO/Al_2O_3 > Au(a)/Al_2O_3 > Au/MnO_x/Al_2O_3 \gg Au(b)/Al_2O_3$, and (ii) the order in H_2 oxidation activity is $Au/MgO/Al_2O_3 \gg Au/MnO_x/MgO/Al_2O_3 \approx Au(a)/Al_2O_3 > Au/MnO_x/Al_2O_3 > Au(b)/Al_2O_3$.

Figure 8 shows the selectivity towards CO_2 (S^{CO_2}) over supported Au catalysts. The results can roughly be divided into three sections. From 25°C to ca. 50°C hardly any H_2 oxidation was found. This was explained by CO, and less likely H_2O, is blocking the sites necessary for H_2 dissociation. Catalysts with high CO oxidation activity have high S^{CO_2}. At temperatures above 50°C the surface coverage of CO becomes that low that it no longer poisons H_2 oxidation. This transition stage is marked by a decrease in E_a for H_2 oxidation and initiates an accelerated O consumption by H_2 at the expense of CO_2 formation, and so lowering S^{CO_2}. From about 300°C S^{CO_2} is increasing again. Though the origin of this behavior is not clear, a possible explanation might be that at these high temperatures the residence time of hydrogen, as a result of a

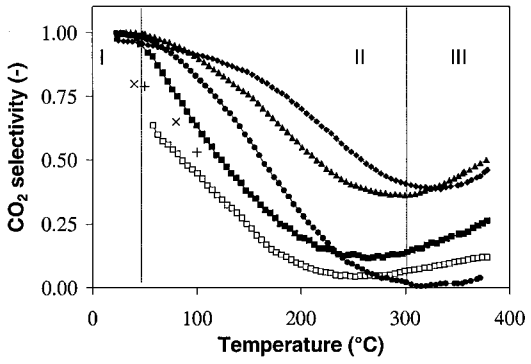

FIG. 8. CO_2 selectivity versus temperature (°C) of $Au(a)/Al_2O_3$ (■), $Au(b)/Al_2O_3$ (□), $Au/MnO_x/Al_2O_3$ (●), $Au/MgO/Al_2O_3$ (▲), and $Au/MnO_x/MgO/Al_2O_3$ (◆), in a mixture of H_2, CO, and O_2 (4 : 2 : 1). From the literature: (16) $Au/\alpha\text{-}Fe_2O_3$ (x) and (17) $Au/\gamma\text{-}Al_2O_3$ (+).

low sticking probability or due to fast H–H recombination, suppresses H_2 oxidation activity in favor of CO oxidation, implying higher S^{CO_2}. Another explanation for the observed increase may be the possibility of a water-gas shift reaction significantly operating at elevated temperature (31).

Typical S^{CO_2} reported in other studies (16, 17) are also plotted in Fig. 8. A similar trend in S^{CO_2} was found. However, it should be noted that the experimental conditions used are not the same. The higher values found in our study are somewhat deceiving, since our results were obtained with much lower H_2 partial pressures. Increasing H_2 partial pressure was found to lead to an overall significant lowering in S^{CO_2} over Pt/Al_2O_3, Ru/Al_2O_3, and Rh/Al_2O_3 (7–10). While increasing the O_2 partial pressure did not seem to influence S^{CO_2} over Pt/Al_2O_3 (8) and Au/Al_2O_3 (17) at relatively low temperatures, it is conceivable that a decrease in the $CO : O_2$ ratio below 0.5, i.e., surplus O_2, may reduce the selectivity. Under the experimental conditions used S^{CO_2} in the temperature range of interest (25–100°C) decreases in the order $Au/MnO_x/MgO/Al_2O_3 > Au/MgO/Al_2O_3 > Au(a)/Al_2O_3 > Au/MnO_x/Al_2O_3$ (Fig. 8).

In the following sections the effect of Au particle size, addition of MgO and MnO_x, pretreatment, and influence of H_2O on the performance of the catalysts are discussed.

4.2. Modification of Au/Al_2O_3 by Addition of MgO and MnO_x

It has generally been accepted that the Au particle size has a large influence on the activity of Au catalysts (12, 13, 32). Therefore, it is very difficult to isolate all possible effects caused by addition of MO_x when the average Au particle sizes of the corresponding catalysts also differ. The oxidation activity of supported Au catalysts should therefore be compared with extreme care. For example, depositing Au onto MgO/Al_2O_3 resulted in (much) smaller Au particles than obtained for Au/Al_2O_3 and $Au/MnO_x/Al_2O_3$. It is clear that addition of MgO is beneficial for obtaining small Au particles with a rather narrow and reproducible particle size distribution. This result is consistent with data reported in the literature (33–35). Bethke and Kung (17) found that addition of Mg citrate during preparation of Au/Al_2O_3 yielded catalysts with smaller Au particles. They ascribe this to the ability of citrate ligands to break up $Au(OH)_3$ clusters in the solution. However, traces of MgO present after oxidation may also stabilize small Au particles. $Au/MgO/Al_2O_3$ exhibits higher CO oxidation activity than Au/Al_2O_3 and $Au/MnO_x/Al_2O_3$, which contain significantly larger Au particles. Thus, the role of MgO might merely be to stabilize small Au particles throughout the preparation and oxidation experiments. On the other hand, both $Au/MgO/Al_2O_3$ and $Au/MnO_x/MgO/Al_2O_3$ were found to have significantly different CO oxidation activities, whereas the average Au particle size was found to be quite similar. Therefore, the role of MnO_x cannot solely be a stabilizing effect on the Au particle size. It is suggested that MnO_x is able to activate O_2 via a Mars and van Krevelen type mechanism (36):

$$\mathrm{Mn{-}O + CO_{ads} \rightarrow Mn{-}\square + CO_2} \quad [1a]$$

$$\mathrm{Mn{-}\square + O_2 \rightarrow Mn{-}O + O^*_{ads}} \quad [1b]$$

$$\mathrm{O^*_{ads} + Mn{-}\square \rightarrow Mn{-}O} \quad [1c]$$

$$\mathrm{O^*_{ads} + CO_{ads} \rightarrow CO_2} \quad [1d]$$

In this model CO is adsorbed on Au and at the Au/MO_x perimeter. It reacts with O from MnO_x, probably along the border with the Au particles [1a]. This O is then replenished by O_2 from the gas phase [1b]. The activated O^* can react with either another O-vacancy [1c] or a second CO molecule [1d].

4.3. Effect of Catalyst Pretreatment on the CO Oxidation Activity

After pre-reduction all catalysts showed improved initial CO oxidation activity. This improvement was most pronounced for catalysts containing MnO_x. Previous studies revealed similar changes in catalytic activity upon addition of other reducible MO_x (37). This behavior can be explained by the ample presence of O-vacancies directly after reduction. During the first heating stage the number of O-vacancies is high, but will decrease as the reaction proceeds. Subsequently, a decrease in activity of the catalysts is observed between the first and the following runs (Fig. 2a). A similar effect can also occur at high conversions in O_2 rich mixtures. To test this hypothesis, reactions were also carried out after oxidative pretreatment of the catalysts. Indeed the initial CO oxidation activity during the first run was somewhat suppressed (Table 5), and the catalyst only gained activity after the first heating stage in the presence of a reducing agent (CO).

Other explanations for the observed differences in initial activity may be that after oxidative pretreatment Au is partly oxidized or is covered by MnO_x. In both cases the amount of adsorbed CO, relevant for the reaction, decreases. From FTIR experiments it can be concluded that CO on metallic Au (ca. 2100 cm^{-1}) is essential to obtain high initial CO oxidation activity (Fig. 6b). After pre-oxidation this band shifts to higher wavenumbers and decreases in intensity, especially for MnO_x comprising catalysts (Fig. 6a).

4.4. *Influence of H_2O*

The effect of H_2O on the CO oxidation activity over supported Au catalysts have been reported previously. Haruta *et al.* (18) found an increase in CO oxidation rate over Au/α-Fe_2O_3 when H_2O was introduced. Boccuzzi and Chiorino (38) also noticed a positive influence of H_2O on the performance of Au/TiO_2 at low temperatures, whereas Bollinger and Vannice (28) reported a detrimental effect over the same catalyst at room temperature. Cunningham *et al.* (39) studied the influence of moisture on Au/$Mg(OH)_2$. While H_2O was found to enhance the oxidation rate at 170°C on Au/$Mg(OH)_2$, the enhancement diminished with decreasing temperature, until it became a poison below 50°C. Moreover, under dry conditions a negative E_a was found for CO oxidation over Au/$Mg(OH)_2$. Because Mozurkewich *et al.* (40) proposed that "negative E_a" in gas-phase CO oxidation involves a radical HOCO species it was suggested that the reaction over Au/$Mg(OH)_2$ proceeds through the direct interaction of adsorbed CO with hydroxyl radicals present at the interface between Au and the support. However, the authors could not explain why this model only appears to be valid under dry conditions, and why H_2O acts as a poison at temperatures below 50°C, while hydroxyl groups (stable just at low T) seem to be necessary for the reaction to proceed.

In our studies reported in this paper only Au/MnO_x/Al_2O_3 experienced a negative influence of H_2O addition on the oxidation activity at room temperature. The CO oxidation rates over the other catalysts were enhanced (Fig. 7). Heating the catalysts resulted in a corresponding change in activity; Au/MnO_x/Al_2O_3 gained activity while the other catalysts became less active, as if the effect of H_2O was reversed by the heat treatments. Consecutive H_2O pulses show the reproducibility of this behavior. The negative influence of H_2O on the CO oxidation activity of Au/MnO_x/Al_2O_3 may originate from poisoning of the O-vacancies in MnO_x. If H_2O blocked CO adsorption sites on Au, none of the catalysts studied would benefit from the presence of H_2O. On the contrary, an improved activity was observed for MgO containing catalysts. These observations are consistent with a second reaction pathway in which OH groups on MgO can provide O needed for CO oxidation (39). It also might be that H_2O causes reconstruction of the (smallest) Au particles and may so engender an altered reactivity. Clearly, more studies are needed to understand the effects of H_2O addition.

Liu *et al.* (41, 42) ruled out the existence of a Mars and van Krevelen mechanism for CO oxidation over Au/$Ti(OH)_4$ and Au/$Fe(OH)_3$ at room temperature based on oxygen isotope exchange studies. They proposed a model in which CO adsorbed on Au metallic particles and O_2^- adsorbed on oxygen vacancies at the oxide surface adjacent to the Au particles are responsible for low-temperature CO oxidation. However, the existence of such a superoxide species has not yet been demonstrated.

4.5. *H_2 Oxidation and the Oxidation of CO in the Presence of H_2*

Unsupported Au was found to catalyze the $H_2 + O_2$ reaction preferentially over CO oxidation (43). However, over well-dispersed Au deposited on MO_x the H_2 oxidation activity was found to be inferior to that of CO oxidation (13–15). Moreover, the presence of H_2 in the reactant flow at room temperature slightly influenced the conversion of CO over Au/MnO_x/Al_2O_3 negatively, whereas the CO oxidation activity of Au/MgO/Al_2O_3 was found to benefit considerably from the presence of H_2 (Fig. 4). At low temperatures the performance of Au/Al_2O_3 and Au/MnO_x/MgO/Al_2O_3 in CO oxidation seemed to be largely unaffected.

During H_2 oxidation experiments hysteresis was found (Fig. 3a). This behavior may well be explained by self-poisoning due to accumulation of H_2O on the surface under ambient conditions. In the heating branch H_2O may block the sites necessary for the dissociation of H_2, thus inhibiting further oxidation. In the cooling branch the H_2O formed largely leaves the surface immediately, leaving enough sites for the reaction to proceed. The absence of hysteresis when CO is present is probably due to the fact that adsorbed CO is interfering with the formation of H_2O. Therefore, only traces of H_2O are expected to be present on the surface at low temperatures. The interference of CO with the oxidation of H_2 at low temperatures is also supported by the decrease in E_a for H_2 oxidation found at temperatures above 67–118°C, the exact temperature depending on the composition of the catalyst (Fig. 5). The high-temperature E_a may be the "true" one, and the low-temperature value may be the true one plus the desorption energy of CO. The absence of change in E_a observed for H_2 oxidation over Au/MnO_x/MgO/Al_2O_3 might point out that on this catalyst the sites necessary for H_2 dissociation are not completely blocked by CO at low temperature. Kahlich *et al.* (16) reported an E_a of 50 kJ mol^{-1} for H_2 oxidation in the presence of CO over Au/α-Fe_2O_3. Although this value agrees with data found for the low temperature branch on our catalysts, the authors did not find evidence for a change in E_a at low temperatures as we did. However, this may be related to the much larger H_2 partial pressure used in their

studies. Currently the influence of CO on H_2 dissociation over supported Au catalysts is studied in more detail. Preliminary results show indeed a poisoning effect of CO on H_2 dissociation.

The presence of H_2 in the feed was found to cause similar changes in CO oxidation activity as H_2O. Therefore, it is not inconceivable to assume that hydrogen is partly present as H_2O or surface OH. This becomes even more plausible, since all catalysts showed considerable H_2 oxidation activity at room temperature (Fig. 3b). Figure 4 shows, however, that H_2 oxidation is inhibited below 50°C when CO is present in the feed. This might be due to the fact that CO competitively adsorbs on special sites, which are necessary to activate H_2. Since CO is only weakly adsorbed on Au, at room temperature probably already a small amount of H_2 can get to the surface and react. Traces of surface OH groups and H_2O thus formed may be sufficient to bring about the differences in activity.

5. CONCLUSIONS

The presence of highly dispersed MgO reduces the average Au particle size, and therefore increases both the CO and H_2 oxidation rates. The presence of MnO_x also increases the oxidation activity by supplying active O, possibly via Mars and van Krevelen redox cycles.

H_2O reversibly alters the CO oxidation activity at ambient temperature. Catalysts containing small Au particles benefit from the presence of H_2O during the oxidation of CO. A possible explanation is that surface OH groups, originating from H_2O, are reactive towards CO, or assist in activation of O_2. This effect was most pronounced with catalysts containing MgO. On the other hand, H_2O was found to poison $Au/MnO_x/Al_2O_3$, the activity of which is mainly attributed to Mars and van Krevelen redox cycles, probably by effectively blocking necessary O-vacancies.

Supported Au catalysts with intrinsically high CO oxidation capacity at ambient temperature can remove CO selectively from H_2 containing gas mixtures at low temperatures. The presence of CO even suppresses H_2 oxidation below 50°C. However, at higher temperature S^{CO_2} decreases in favor of H_2 oxidation. No indication of CH_3OH or CH_4 formation was found.

To obtain the best performance in CO oxidation, supported Au catalysts need to be reduced in either H_2 or CO. Thus, it is concluded that metallic Au is the active species for the oxidation of CO. The main role of Au is to adsorb CO and possibly assist in the activation of O_2 near the Au/oxide interface, via O-vacancies or surface OH groups on oxide.

ACKNOWLEDGMENTS

The authors thank Dr. P. J. Kooyman of the National Centre for High Resolution Electrón Microscopy, Delft University of Technology, Delft, The Netherlands, for performing the HRTEM measurements. This work has been performed under the auspices of NIOK, the Netherlands Institute for Catalysis Research. This is Lab Report UL 00-2-08.

REFERENCES

1. Daimler-Benz, "NECAR II—Driving without Emissions," Daimler-Benz, Stuttgart, 1996.
2. Hohlein, B., von Andrian, S., Grube, T., and Menzer, R., *J. Power Sources* **86**, 243 (2000).
3. Freni, S., Calogero, G., and Cavallaro, S., *J. Power Sources* **87**, 28 (2000).
4. Mann, R. F., Amphlett, J. C., and Peppley, B. A., *Front. Sci. Ser.* **7**, 613 (1993).
5. Gottesfeld, S., and Pafford, J., *J. Electrochem. Soc.* **135**, 2651 (1988).
6. Oetjen, H.-F., Schmidt, V. M., Stimming, U., and Trila, F., *J. Electrochem. Soc.* **143**, 3838 (1996).
7. Watanabe, M., Uchida, H., Igarashi, H., and Suzuki, M., *Chem. Lett.*, 21 (1995).
8. Kahlich, M. J., Gasteiger, H. A., and Behm, R. J., *J. Catal.* **171**, 93 (1997).
9. Oh, S. H., and Sinkevitch, R. M., *J. Catal.* **142**, 254 (1993).
10. Brown, M. L., Green, A. W., Cohn, G., and Andersen, H. C., *Ind. Eng. Chem. Res.* **52**, 841 (1960).
11. Lin, S. D., Bollinger, M., and Vannice, M. A., *Catal. Lett.* **17**, 245 (1993).
12. Haruta, M., Tsubota, S., Kobayashi, T., Kageyama, H., Genet, M., and Delmon, B., *J. Catal.* **144**, 175 (1993).
13. Haruta, M., Yamada, N., Kobayashi, T., and Iijima, S., *J. Catal.* **115**, 301 (1989).
14. Torres Sanchez, R. M., Ueda, A., Tanaka, K., and Haruta, M., *J. Catal.* **168**, 125 (1997).
15. Okumura, M., Nakamura, S., Tsubota, S., Nakamura, T., Azuma, M., and Haruta, M., *Catal. Lett.* **51**, 53 (1998).
16. Kahlich, M. J., Gasteiger, H. A., and Behm, R. J., *J. Catal.* **182**, 430 (1999).
17. Bethke, G. K., and Kung, H. H., *Appl. Catal. A* **194**, 43 (2000).
18. Haruta, M., Ueda, A., Tsubota, S., and Torres Sanchez, R. M., *Catal. Today* **29**, 443 (1996).
19. Grisel, R. J. H., Kooyman, P. J., and Nieuwenhuys, B. E., *J. Catal.* **191**, 430 (2000).
20. Scherrer, P., and Nachr. K. Ges. Wiss., Göttingen 98 (1918).
21. Lee, S-J., Gavriilidis, A., Pankhurst, Q. A., Kyek, A., Wagner, F. E., and Yeung, K-L., *Asia-Pacific Chem. React. Eng. Symp.* **1** (1999).
22. Haruta, M., *Catal. Today* **36**, 153 (1997).
23. Haruta, M., *Catal. Surv. Jpn.* **1**, 61 (1997).
24. Kozlov, A. I., Kozlova, A. P., Liu, H., and Iwasawa, Y., *Appl. Catal. A* **182**, 9 (1999).
25. Bond, G. C., and Thompson, D. T., *Catal. Rev. Sci. Eng.* **41**, 319 (1999).
26. Dekkers, M. A. P., Lippits, M. J., and Nieuwenhuys, B. E., *Catal. Lett.* **56**, 195 (1998).
27. Dekkers, M. A. P., Lippits, M. J., and Nieuwenhuys, B. E., *Catal. Today* **54**, 381 (1999).
28. Bollinger, M. A., and Vannice, M. A., *Appl. Catal. B* **8**, 417 (1996).
29. Boccuzzi, F., Chiorino, A., Tsubota, S., and Haruta, M., *Catal. Lett.* **29**, 225 (1994).
30. Minicò, S., Scirè, S., Visco, A., and Galvagno, S., *Catal. Lett.* **47**, 273 (1997).
31. Andreeva, D., Idakiev, V., Tabakova, T., Andreev, A., and Giovanoli, R., *Appl. Catal. A* **134**, 275 (1996).
32. Valden, M., Lai, X., and Goodman D. W., *Science* **281**, 1647 (1998).
33. Blick, K., Mitrelias, T. D., Hargreaves, J. S. J., Hutchings, G. J., Joyner, R. W., Kiely, C. J., and Wagner, F. E., *Catal. Lett.* **50**, 211 (1998).
34. Vogel, W., Cunningham, D. A. H., Tanaka, K., and Haruta, M., *Catal. Lett.* **40**, 175 (1996).

35. Cunningham, D. A. H., Vogel, W., Kageyama, H., Tsubota, S., and Haruta, M., *J. Catal.* **177**, 1 (1998).
36. Mars, P., and van Krevelen, D. W., *Chem. Eng. Sci. Spec. Suppl.* **3**, 41 (1954).
37. Grisel, R. J. H., and Nieuwenhuys, B. E., *Catal. Today* **64**, 69 (2001).
38. Boccuzzi, F., and Chiorino, A., *J. Phys. Chem. B* **104**, 5414 (2000).
39. Cunningham, D. A. H., Vogel, W., and Haruta, M., *Catal. Lett.* **63**, 43 (1999).
40. Mozurkewich, M., Lamb, J. J., and Benson, S. W., *J. Phys. Chem.* **88**, 6435 (1984).
41. Liu, H., Kozlov, A. I., Kozlova, A. P., Shido, T., Asakura, K., and Iwasawa, Y., *Phys. Chem. Chem. Phys.* **1**, 2851 (1999).
42. Liu, H., Kozlov, A. I., Kozlova, A. P., Shido, T., Asakura, K., and Iwasawa, Y., *J. Catal.* **185**, 252 (1999).
43. Iizuka, Y., Fujiki, H., Yamauchi, N., Chijiiwa, T., Arai, S., Tsubota, S., and Haruta, M., *Catal. Today* **36**, 115 (1997).